# Comparison of mining-induced seismicity within a footwall fault between overhand and underhand stoping methods

Atsushi Sainoki and Hani S. Mitri
*Department of Mining and Materials Engineering, McGill University, Montreal, Quebec, Canada*

ABSTRACT
The behaviour of faults in underground mines has been attracting much attention from rock mechanics specialists. In this study, a comparison between overhand and underhand sublevel stoping methods is made whilst focusing on the static and dynamic behaviour of a footwall fault intersecting with a steeply dipping orebody. A mine-wide numerical model representing the geological features is constructed. Using the model, static analyses are performed to extract stopes in the orebody. It is found from the result that the stope extraction with the underhand mining method produces more seismically active conditions on the fault, compared to the overhand method. Then, fault-slip is simulated with an instantaneous change of the friction law from static to dynamic. The analysis indicates that there is no significant difference in the intensity of near-field ground motion between fault-slips induced by the stope extraction with the two mining methods.

RÉSUMÉ
Le comportement des failles dans les mines sous-terraines attire actuellement l'attention des spécialistes en mécanique des roches. Dans cette étude, l'extraction descendante d'un gisement à fort pendage par l'abattage de chantiers remblayés est comparée à l'extraction ascendante du même gisement. Le comportement statique et dynamique d'une faille dans l'éponte inférieure est étudié. Un modèle numérique de la mine représentant les structures géologiques a été construit. Des analyses statiques ont été conduites avec le modèle pour abattre les chantiers. Il est observé que l'extraction descendante du gisement génère des conditions plus sismiquement actives dans la faille que l'extraction ascendante. Ensuite, le glissement de la faille est simulé en changeant instantanément son coefficient de friction de statique à dynamique. L'analyse indique qu'il n'y a pas de différence significative entre l'intensité des mouvements de sol en champ proche entre les glissements de faille induits par les 2 méthodes d'extraction.

## 1 INTRODUCTION

Seismic events taking place in underground mines are serious issues as severe damage to underground openings and equipment is often encountered due to the propagation of seismic waves. It is commonly recognized that pre-existing faults can be the cause of large seismic events (Ortlepp, 2001; Alber and Fritschen, 2011; Sainoki and Mitri, 2014a). Ortlepp (2001) characterizes the magnitude of seismic events according to its source mechanism. It is then shown that the magnitude of seismic events produced by fault-slip ranges from 2.5 to 5.0, which can cause significantly high peak particle velocity, even if the distance between the source location and the underground opening is large (Hedley, 1992). Hence, it is of significant importance to investigate and analyze the effect of mining activities on the behaviour of faults in underground mines.

To date, a number of studies have been undertaken for better understanding of the behaviour of faults in relation to mining activities. For instance, calibration of mechanical properties of fault and/or shear zones is conducted (Potvin et al., 2010; Hofmann and Scheepers, 2014; Sainoki and Mitri, 2014b). For the calibration, seismic moment is commonly used as it is readily computed from analysis results. Sjöberg et al (2012) examine several different mining sequences after carrying out sensitivity analysis with respect to fault mechanical properties. Sainoki and Mitri (2014a, c, d) investigate the dynamic behaviour of fault-slip caused by mining activities, assuming that shearing of fault surface asperities is the source mechanism of fault-slip. As fault-slip is a dynamic phenomenon producing seismic waves, it is indispensable to gain deep knowledge of its dynamic behaviour. Owing to the studies, the effect of fault surface properties, such as roughness and slip-weakening distance, on seismic source parameters of fault-slip is clarified.

In addition to the numerical simulations mentioned above, analytical and empirical approaches to understanding the characteristics of mining-induced seismic events have been intensively undertaken by many researchers. McGarr (2002) proposes an equation to estimate peak particle velocity (the severity of ground motion), using the constraint of seismic efficiency of fault-slip that takes place in underground mines (McGarr 1999). Given that the constraint is valid, damage to rockmass induced by seismic waves can be roughly estimated as a function of particle velocity. Empirical relations between damage and seismic source parameters are summarized by Hedley (1992).

As described above, significant efforts have been made for the study of mining-induced fault-slip. However, to author's knowledge, the behaviour of a fault intersecting with an orebody or a mine opening has not yet been studied sufficiently, although such situations are often encountered in underground mines (White, 1999; Ortlepp, 2001). Additionally, it is still unclear how the

stability of geological structures changes when a different mining method is applied. Considering the fact, in the present study, numerical simulations are carried out to examine the stability of a fault intersecting with a steeply dipping orebody. Two mining directions, namely bottom-up and top-down, are employed to mine out the orebody, and the results are compared in terms of seismic moment of fault-slip induced by the mining activities. Furthermore, the dynamic behaviour of the fault during fault-slip is analyzed with dynamic analyses, focusing on near-field particle velocity.

## 2 MODEL DESCRIPTION

In the present study, Rhino 5.0 (Robert McNeel & Associate) is employed to construct 3D wireframes representing a steeply dipping orebody intersecting with a footwall fault. As explained in the previous section, the present study focuses on the geological structure. The constructed wireframes are discretized into tetrahedral meshes with KUBRIX (Itasca, 2009) for carrying out numerical analysis. The discretized model is analyzed with FLAC3D code (Itasca, 2009), which employs an explicit finite difference method. In this section, detailed descriptions on the model and the mining sequences investigated are provided.

### 2.1 Model Geometry

Fig. 1 illustrates an isometric view of the constructed numerical model. As can be seen, the height, width, and length of the model are 700 m, 400 m, and 650 m, respectively. The dimensions of the model are determined in order to minimize the effect of the model boundaries on the stress and deformation of the geological structures, considering realistic computation time. Mesh density is varied, so that coarse meshes are generated in the vicinity of the model boundaries, and the mesh density increases towards the inner part, where the geological structures are modelled. The total numbers of zones and grid points in the model are 863284 and 146086, respectively.

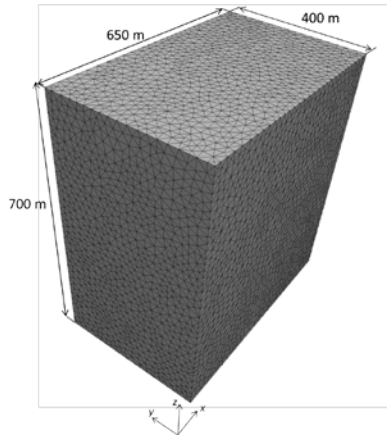


Figure 1. Isometric view of a numerical model analyzed

Fig. 2 represents the geological structures modelled inside the mine-wide model. As shown in the figure, the orebody steeply dips at 80°; the fault dips at 70° and intersects with the orebody. The fault runs parallel to the orebody, and its strike coincides with the y-direction. Fig. 2 explicitly shows that the meshes generated for the orebody and the fault are significantly smaller than those on the model boundaries in Fig. 1, thus making it possible to analyze stress and deformation in those areas more accurately. The lengths of the orebody and the fault are 200 m and 300 m, respectively. The height of the fault is 600 m. Mining blocks (stopes) are modelled inside the orebody and extracted in accordance with mining sequences representing the two mining methods. The simulated mining sequences are explained in the next section.

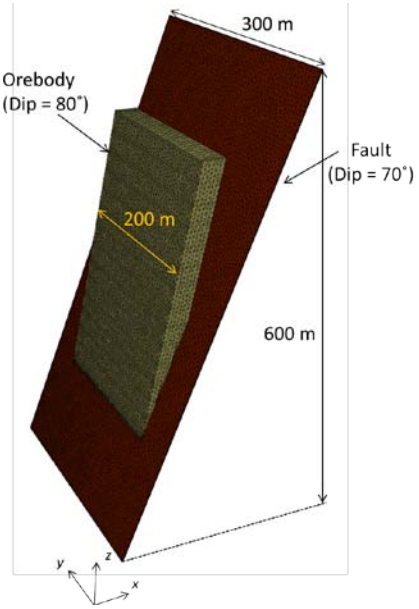


Figure 2. Geological structures modelled inside of the numerical model shown in Fig. 1

### 2.2 Mining sequence

In the present study, a comparison of two mining directions is conducted, namely bottom-up and top-down mining. The numbers shown in Fig. 3 represent mining sequences according to the two mining directions. As can be seen in the figure, in the case of the bottom-up mining, stopes are extracted in sequence from the bottom of the orebody going up. In practice methods such overhand cut-and-fill and sublevel open stoping employ a bottom-up mining direction. In contrast, top-down mining starts from the top of the orebody going down. This is commonly associated with undercut and fill, and underhand open stoping methods. For both mining sequences, stopes are mined out from hanging wall to foot wall on each level. The stopes modelled in the present study are 25 m high and 10 m wide as shown in the figure. The length of the stope is the same as that of the orebody, i.e., 200 m. The height and width of the stope fall into the reasonable range of stope dimensions designed in the Canadian Shield (Zhang and Mitri, 2008), while the length is considerably larger than that of ordinary stopes. It is to be noted, however, that the purpose of this study is to

examine the difference in the stability of the fault between the two mining directions. As the main discrepancy between the two scenarios is the mining direction (see Fig. 3), the effect of stope strike length can be ignored as long as the same stope length is used for the two cases. It should be noted that, during the simulations of mining sequences, backfill is applied after extracting each stope.

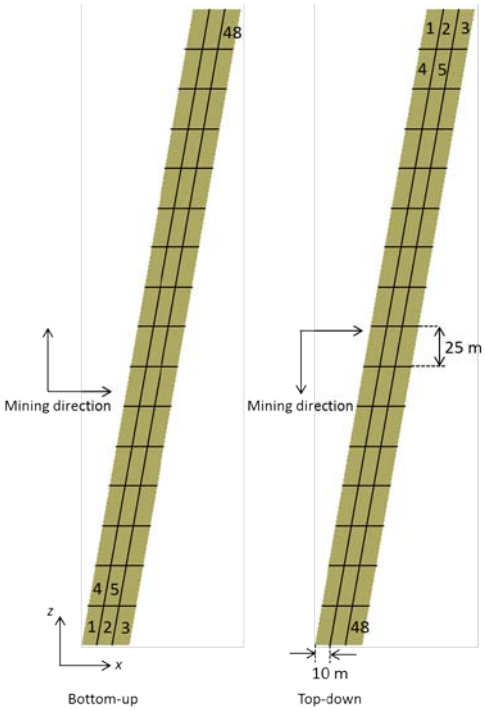


Figure 3. Schematic illustration of mining directions studied

## 2.3 Mechanical Properties of Rockmass

The mechanical properties of the hanging wall, footwall, and orebody in the constructed numerical model are determined based on the case study conducted by Henning (1998) in which the author investigates the rockmass mechanical properties at the Bousquet 2 Mine, Canada. The hanging wall, orebody, and footwall in the mine consist of Rhyolite Tuff, massive Sulphide, and Rhyolite, respectively. The rockmasses in the mine were characterized with RMR developed by Bieniawski (1976). Specifically, the RMR for the hanging wall, orebody and footwall were estimated to be 50, 75, and 55, respectively. The mechanical properties of rock specimens estimated with laboratory experiments are converted to those for in-situ rockmass, taking into account RMR.

Table 1 shows the estimated mechanical properties. In the table, $E$, $C$, $\phi$, $v$, $\gamma$, $\sigma_T$, and $\psi$ denote modulus of elasticity, cohesive strength, friction angle, Poisson's ratio, unit weight, tensile strength, and dilation angle, respectively. Note that tensile strength is assumed to be one-tenth of uniaxial compressive strength (Tesarik et al., 2003) and that dilation angle is assumed to be one-fourth of friction angle (Hoek and Brown, 1997). Regarding backfill, the same mechanical properties as those used by Zhang and Mitri (2008) are applied.

Table 1. Mechanical properties of the rockmass and backfill

| | E (GPa) | C (MPa) | $\phi$ (˚) | $v$ | $\Gamma$ (kN/m$^3$) | $\sigma_T$ (MPa) | $\Psi$ (˚) |
|---|---|---|---|---|---|---|---|
| HW[1] | 31 | 2.6 | 38 | 0.21 | 25.5 | 1.1 | 9.3 |
| Ore | 115 | 11.5 | 48 | 0.1 | 25.5 | 5.9 | 12.0 |
| FW[2] | 49 | 4.3 | 39 | 0.15 | 25.5 | 1.8 | 9.5 |
| BF[3] | 2.5 | 0.1 | 35 | 0.35 | 23.0 | N/A | 0.0 |

[1]hanging wall
[2]footwall
[3]backfill

## 2.4 Mechanical Model for Fault

In the present study, the fault is modelled with ubiquitous joint models. As shown by Cappa and Rutqvist (2011), ubiquitous joint models behave in the almost same way as interface models when used to model a fault. The employed ubiquitous joint model uses the classical Mohr-Coulomb failure criterion while assuming ubiquitous joints with the same dip angle and direction as those for the fault. The friction angle of the ubiquitous joint is assumed to be 30˚. According to Barton and Choubey (1977), the basic friction angle of a typical rock joint falls into a range from 21˚ to 38˚. The adopted friction angle in the present study is an intermediate value in the range.

The modulus of elasticity for the ubiquitous joint model is assumed to be one-tenth of that for the rockmass in the hanging wall. It is commonly recognized that fault zones have low stiffness due to cracks and fractures, but the degree to which the stiffness of rockmass within fault zones decreases is dependent upon a number of factors, such as the number of fractures. More importantly, the primary objective of this study is the comparison of the two mining methods. Hence, the estimated properties of the fault are deemed sufficient for this study.

## 2.5 In-situ Stress State

In this section, in-situ stress state applied to the mine-wide model is explained. The vertical in-situ stress, $\sigma^o_v$, which is in the z-direction in Fig. 1, is determined by the overburden as:

$$\sigma^o_v = \gamma H \quad [1]$$

where $H$ is the depth below the ground surface. In the present study, the top boundary of the mine-wide model is assumed to be 1500 m below the ground surface. For horizontal stresses, equations proposed by Diederichs (1999) are employed. The equations are expressed as:

$$k_{max} = 1 + 25/H^{0.5} \quad [2]$$

$$k_{min} = 1 + 8/H^{0.5} \quad [3]$$

where $k_{max}$ and $k_{min}$ represent the maximum and minimum horizontal-to-vertical stress ratios, respectively. Note that $H$ in Equations 2 and 3 is in metres. Diederichs (1999) obtained the equations based on the stress-depth

relationships estimated by Arjang and Herget (1997). The obtained equations adequately represent the characteristics of stress state in the Canadian Shield. In the present study, it is assumed that the maximum horizontal stress acts in the direction perpendicular to the strike of the orebody.

## 3 STATIC ANALYSIS

The stability of the fault is examined with static analyses, in which the stopes in the orebody are extracted in accordance with the mining sequences as per the mining direction. In this section, first, the analysis procedure for the static analysis is explained. Then, the results obtained from the static analysis are evaluated in terms of relative shear displacements taking place on the fault during the mining sequences.

### 3.1 Analysis procedure

Fig. 4 schematically illustrates analysis procedure for the static analyses. As the first step, initial stress state is simulated in the model with a static analysis while applying the vertical and horizontal stresses obtained from Equations 1 to 3 to the zones. The model boundaries are fixed in the direction perpendicular to the boundaries.

Based on the initial stress state, the mining sequences are simulated, whereby the stopes in the orebody are extracted and backfilled according to the numbers in Fig. 3. During the static analyses to extract stopes, relative shear displacements on the fault are monitored to assess the effect of the stope extraction on the stability of the fault.

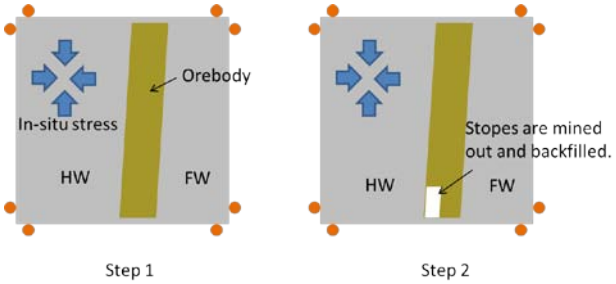


Figure 4. Analysis procedure for static analysis

### 3.2 Results and discussion

The monitored shear displacements during the mining sequences are used to compute seismic moment, which is a widely-used parameter to evaluate the severity of seismic event (Domański and Gibowicz, 2008; Sjöberg et al., 2012). Seismic moment is calculated from the following equation:

$$M_o = GDA \quad [4]$$

where $G$, $D$, and $A$ represent shear modulus, average relative shear displacement increment, and area where sliding takes place, respectively. Seismic moment is computed based on the increments of relative shear displacements after extracting each stope.

Fig. 5 shows the cumulative values of seismic moment computed with the method. The cumulative seismic moment indicates the severity of mining-induced seismicity that takes place on the fault in the course of the mining sequences. It is to be noted that the numbers of horizontal axis in the figure coincide with those in Fig. 3. It is found from Fig. 5 that top-down mining induces less seismic events, compared to the bottom-up mining, until the mining sequence reaches the 16$^{th}$ step. Interestingly, afterwards, the intensity of seismicity suddenly increases for top-down mining, while there is no noticeable change for bottom-up mining. The sudden increase in cumulative seismic moment for top-down is reasonable since the locations of stopes mined out approach the fault as the mining sequence proceeds. In contrast, in the case of bottom-up mining method, although extracted stopes are situated close to the fault at the beginning of the mining sequence, the distance between the extracted stopes and the fault increases as the mining sequence proceeds.

The reason for the ultimate cumulative seismic moment for top-down method is larger than that for the bottom-up method can be deduced from the study (Sainoki and Mitri, 2014a). According to the study, stope extraction tends to cause shear displacements in the area of a fault above the extracted stope. In the case of top-down mining, when a stope is extracted, it is assumed that the area of the fault above the extracted stope has already become burst-prone, i.e., shear stress acting on the fault approaches the failure criterion. This is because the mining sequence proceeds towards the bottom of the orebody. On the other hand, when bottom-up mining method is employed, the area of the fault above stopes to be extracted is not significantly affected by the past mining activities.

Fig. 6 shows cumulative relative shear displacements after all the stopes are extracted for two mining directions simulated. Obviously, the relative shear displacements on the fault that take place during the mining sequence as per top-down mining are greater than those for bottom-up mining. The result is in agreement with that in Fig. 5.

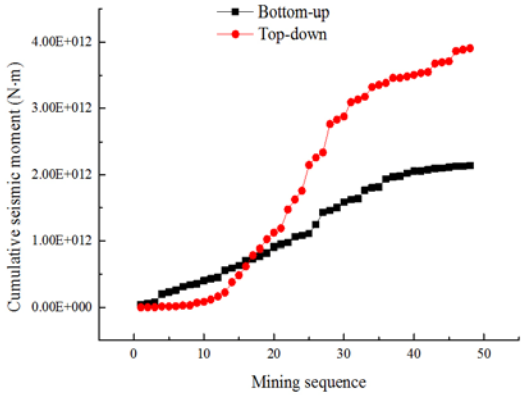


Figure 5. Cumulative seismic moment for the mining directions simulated

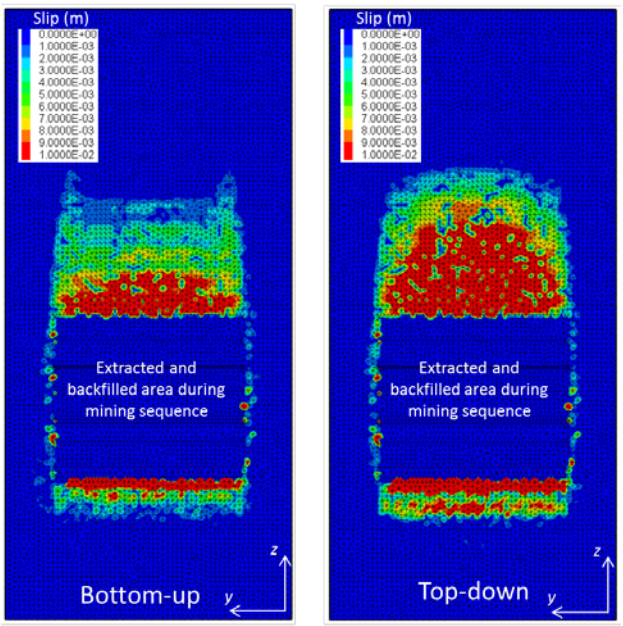


Figure 6. Relative shear displacements on the fault after all the stopes are extracted with the bottom-up (left) and top-down mining directions

## 4 DYNAMIC ANALYSIS

Dynamic analyses are performed in order to investigate the difference in the dynamic behaviour of the fault during fault-slip between the two mining directions. In this section, first, procedure for the dynamic analyses is explained. After that, the results obtained from the dynamic analyses are evaluated in terms of near-field particle velocity.

### 4.1 Analysis Procedure

Fig. 7 shows the procedure to simulate fault-slip in dynamic conditions. As shown in the figure, the dynamic analyses are conducted based on the stress state after extracting all the stopes in the orebody with the static analyses. First, the boundary conditions are changed to viscous in order to prevent seismic waves produced by fault-slip simulated in the dynamic analyses from reflecting on the model boundaries.

Then, stress states in all the zones within the fault are examined, and the friction angle is decreased to 15° for the zones where the shear stress acting on the fault reaches the failure criterion. The reduction in the friction angle represents the sudden weakening of the shear strength of the fault as well as the change from static to kinetic friction. As the cause for the sudden decrease in the shear strength, the breakage of fault surface asperities can be considered (Ryder, 1988). Although Sainoki and Mitri (2014b) simulate fault-slip induced by asperity failure on a fault surface with Barton's shear strength model (1977), in the present study, it is assumed that the weakening behaviour caused by the shearing of surface asperities is represented solely with the decrease in the friction angle. Considering the purpose of this study, the employed simulation technique is deemed sufficient. Hofmann and Scheepers (2011) employ a similar method to simulate fault-slip.

Afterwards, dynamic analyses are carried out. The time step used during the dynamic analysis is automatically optimized with FLAC3D code, considering the volume and face area of zones and the mechanical property. The actual time step used in the analyses is $9.6\times10^{-6}$ s. During the dynamic analyses, the stress state of zones within the fault is continuously checked at a time interval of $1.0\times10^{-4}$ s, and if there are additional zones where the shear stress reaches the maximum shear strength, the friction angle is decreased as explained above. The dynamic analysis is continued until 0.03 s. The time was found to be long enough to investigate the dynamic behaviour of the fault during fault-slip.

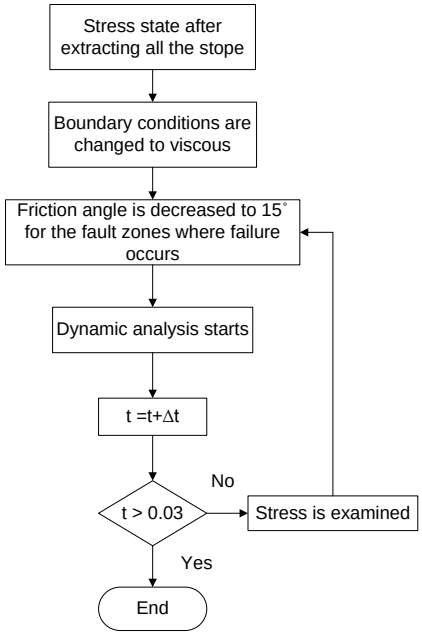


Figure 7. Flowchart for dynamic analysis

### 4.2 Results and Discussion

The results obtained from the dynamic analyses are evaluated in terms of particle velocity on the fault as particle velocity is one of the most important factors associated with damage induced by seismic waves arising from fault-slip. Fig. 8 shows particle velocities on the fault for the two mining scenarios. For both cases, at the beginning of the dynamic analyses, fault-slips start to take place on the upper parts of the fault as well as on the lower parts. This is because the middle of the fault, which intersects with the orebody, is extracted and backfilled during the mining sequences. As shown in Fig. 8, it appears that, in the case of the top-down mining, fault-slip is more severe and takes place in more extensive area at 0.01 s after the onset of the dynamic analysis. This is expected from Fig. 6, which shows that the top-down mining induces more intensive shear displacements on the fault, indicating that the shear stress acting on the fault reaches the failure criterion in more extensive area.

Importantly, the areas colored in red in Fig. 8 indicate that particle velocity is greater than 0.5 m/s. According to the damage threshold with respect to peak particle velocity (Brinkmann et al., 1987), the particle velocity is high enough to cause instability, such as rock falls, along an unlined tunnel, although the particle velocities shown in Fig. 8 are peak values and attenuate as seismic waves propagate through rockmass.

As time elapses, fault-slip extends to larger areas on the fault, but particle velocities decrease on the whole as shown in Fig. 8. In the case of the top-down mining, high particle velocities greater than 0.5 m/s are observed only within a small area at 0.03 s. Excluding the area, particle velocities are less than 0.25 m/s. In the case of the bottom-up mining, interestingly, there are still comparatively large areas with high particle velocities at 0.03 s, although the particle velocities reduce on the whole in the same way.

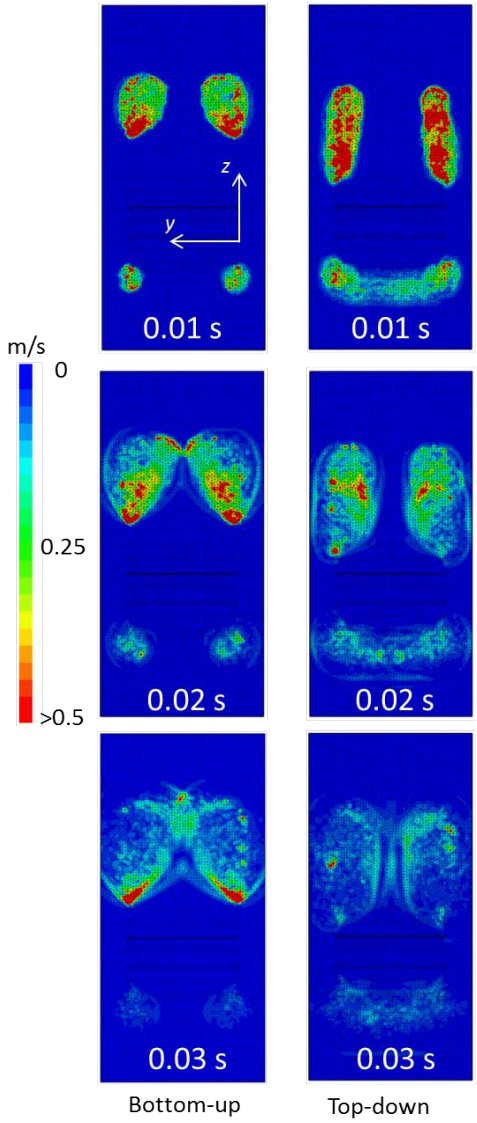


Figure 8. Particle velocity on the fault during dynamic analysis for bottom-up and top-down mining methods

Particle velocities on the cross-section of the mine-wide model during the dynamic fault-slips for the two mining scenarios are shown in Fig. 9. It can be seen from the figure that there is a difference in the intensity of rockmass vibration between the hanging wall and the footwall. This characteristic appears more clearly when top-down mining is employed. For instance, regions with high particle velocities greater than 0.5 m/s are present in the upper part of the hanging wall at 0.01 s, whilst more intense rockmass vibration takes place in the footwall at 0.03 s. Compared to top-down mining, there is no significant difference in particle velocity between the hanging wall and the footwall in the case of the bottom-up mining, although it appears that intense ground motion is about to take place on the hanging wall side. The discrepancy in the intensity of ground motion induced by seismic waves between the hanging wall and the footwall highlights the importance of performing numerical analysis to simulate seismic wave propagation, whereby the intensity of ground motion in the large area can be estimated. Hence, proper measures can be taken, if needed. It thus implies the limitation of the empirical relationship to estimate peak particle velocity induced by seismic waves arising from rockbursts (Hedley, 1992), which takes into account only the distance from a source.

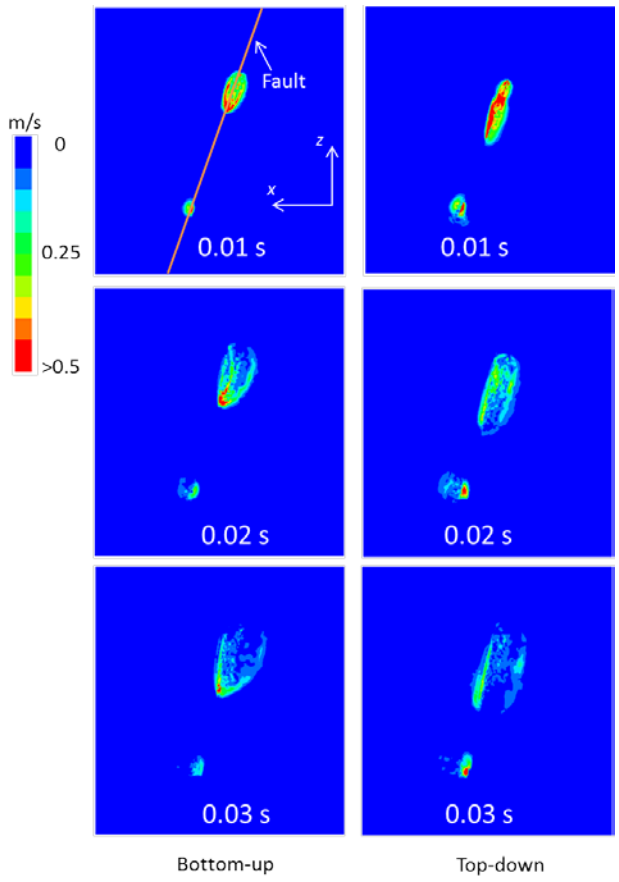


Figure 9. Particle velocity on the cross-section during dynamic analysis for bottom-up and top-down mining methods

In terms of maximum particle velocities taking place on the entire fault, the results reveal that there is no significant difference between the two mining methods. In fact, the observed maximum particle velocities are 2.6 m/s and 2.4 m/s at 0.03 s for the top-down and bottom-up mining methods, respectively. This is reasonable as peak particle velocity induced by fault-slip is a function of the shear wave speed, shear stress acting on the fault, rupture velocity, and shear modulus (McGarr, 2002). For the two mining directions, shear wave speed and shear modulus are the same, and it is assumed that the shear stress acting on the fault would not significantly differ because the same in-situ stress and failure criterion are applied to the model.

## 5 CONCLUSION

The present study compares two mining methods, namely bottom-up and top-down mining, using a numerical model encompassing a steeply dipping orebody that intersects with a footwall fault. Static analyses are performed, in which mining blocks (stopes) in the orebody are extracted in accordance with mining sequences as per the two mining methods. The seismic moment of fault-slip taking place during the mining sequences is computed. The results show that the top-down mining method induces more intense seismicity on the fault than the bottom-up mining method. In addition to the static analyses, dynamic analyses are performed based on the stress states after extracting all the stopes with the two mining methods. During the dynamic analyses, fault-slip is simulated in dynamic conditions with sudden reduction in friction angle, which represents asperity failure on the fault surface and change from static to kinetic friction. The results show that although high particle velocities greater than 0.5 m/s are induced in more extensive area when the top-down mining method is employed, the maximum particle velocity taking place on the fault is almost the same for the two mining methods. Considering the fact that particle velocity is one of the most important factors that determine the severity of damage induced by seismic waves, the results obtained from this study imply that the decision between overhand and underhand sublevel stoping methods should be based on other equally important factors such as state of stress around the stopes leading to potential strainburst and volume of remaining ore at risk, although the top-down mining method might cause more seismicity along nearby faults.

## ACKNOWLEDGEMENTS

This work is financially supported by a grant by the Natural Science and Engineering Research Council of Canada (NSERC) in partnership with Vale Ltd – Sudbury Operations, Canada, under the Collaborative Research and Development Program. The authors are grateful for their support.

## REFERENCES

Alber, M. and Fritschen R. 2011. Rock mechanical analysis of a M1 = 4.0 seismic event induced by mining in the Saar District, Germany. *Geophysical Journal International*, 186: 359-372.

Arjang, B. and Herget, G. 1997. In situ ground stresses in the Canadian Hardrock Mines: An Update, *International Journal of Rock Mechanics and mining Science & Geomechanics Abstracts*, 34: 15.e1-15.e16.

Barton, N. and Choubey, V. 1977. The shear strength of rock joints in theory and practice, Rock Mechanics, 10: 1-54.

Bieniawski, Z.T. 1976. Rock mass classification in rock engineering, *In Exploration for Rock Engineering*, Balkema, Cape Town.

Brinkmann, J.R. 1987. Separating shock wave and gas expansion breakage mechanism, *2nd International Symposium rock fragmentation by blasting*.

Cappa, F. and Rutqvist, J. 2010. Modeling of coupled deformation and permeability evolution during fault reactivation induced by deep underground injection of CO2, International Journal of Greenhouse Gas Control, 5: 336-346.

Diederichs, M.S. 1999. *Instability of hard rockmass: the role of tensile damage and relaxation*, PhD thesis, University of Waterloo, Waterloo, Canada.

Domański, B. and Gibowicz, S.J. 2008. Comparison of source parameters estimated in the frequency and time domains for seismic events at the Rudna copper mine, Poland, Acta Geophysica, 56(2): 324-343.

Hedley, D.G.F. 1992. *Rockburst handbook for Ontario rock mines*, Minister of Supply and Service, Canada.

Henning, J. 1998. *Ground control strategies at the bousquet 2 mine*, Master thesis, McGill University, Canada.

Hoek, E. and Brown, E.T. 1997. Practical estimates of rock mass strength, International Rock Mechanics and Mining Science Geomechanics Abstract, 34(8): 1165-1186.

Hofmann, G.F. and Scheepers, L.J. 2011. Simulating fault slip areas of mining induced seismic tremors using static boundary element numerical modelling, *Mining Technology*, 120(1): 53-63.

McGarr, A. 1999. On relating apparent stress to the stress causing earthquake fault slip, *Journal of Geophysical Research*, 104(B2): 3003-3010.

McGarr, A. 2002. Control of strong ground motion of minig-induced earthquakes by the strength of the seismogenic rock mass, *The Journal of The South African Institute of Mining and Metallurgy*, 225-229.

Ortlepp, W.D. 2001. The behaviour of tunnels at great depth under large static and dynamic pressures, *Tunnelling and Underground Space Technology*, 16: 41-48.

Potvin, Y., Jarufe, J. and Wesseloo, J. 2010. *Interpretation of seismic data and numerical modelling of fault reactivation at El Teniente, Reservas Norte sector*, Mining Technology, 119(3): 175-181.

Sainoki, A. and Mitri, H.S. 2014a. Dynamic behaviour of mining-induced fault-slip, *International Journal of Rock Mechanics and Mining Science*, 66: 19-29.

Sainoki, A. and Mitri, H.S. 2014b. Methodology for the interpretation of fault-slip seismicity in a weak shear zone, *Journal of Applied Geophysics*. 110: 126-134.

Sainoki, A. and Mitri, H.S. 2014c. Dynamic modelling of mining-induced fault-slip with Barton's shear strength model, *International Journal of Rock Mechanics and Mining Science*, 67: 155-163.

Sainoki, A. and Mitri, H.S. 2014d. Effect of slip-weakening distance on selected seismic source parameters of mining-induced fault-slip, *International Journal of Rock Mechanics and Mining Science*, 73: 115-122.

Sjöberg, J., Perman, F., Quinteiro, C., Malmgren, L., Dahner-Lindkvist, C., and Boskovic, M. 2012. Numerical analysis of alternative mining sequences to minimize potential for fault slip rockbursting, *Mining Technology*, 121(4): 226-235.

Tesarik, D.R., Seymour, J.B., and Yanske, T.R. 2003. Post-failure behaviour of two mine pillars confined with back fill, *International Journal of Rock Mechanics and Mining Science,* 40(2):221.

White, B.G. and Whyatt, J.K. 1999. Role of fault slip on mechanisms of rock burst damage, Lucky Friday Mine, Idaho, USA, *2nd Southern African Rock Engineering Symposium, Implementing Rock Engineering Knowledge*, Johannesburg, South Africa.

Zhang, Y. and Mitri, H.S. 2008. Elastoplastic stability analysis of mine haulage drift in the vicinity of mined stopes, *International Journal of Rock Mechanics and Mining Science*, 45: 574-593.